Super-resolved Point Source Tracking Using Birefringent Impulse Response Coding

A. D. Portnoy, J. P. Guo and D. J. Brady

Fitzpatrick Center for Photonics and Communications,
Duke University, Durham, NC 27706 USA
adp4@duke.edu

Abstract

A set of crossed birefringent crystals creates a distributed impulse response. The first moment of the pixel intensity distribution localizes a point source target to a finer accuracy than is possible with a localized impulse response.

Keywords: OCIS codes: (100.6640) Superresolution; (100.2000) Digital image processing

1. Introduction

A conventional approach to point source tracking consists of imaging the target onto a detector plane. The location of the point source can be described by the location of the pixel reading the highest intensity. The resolution in the image plane is limited by the size of the pixels. We present a method to track the location of a point source to a resolution finer than size of the detector pixels. The approach does not require taking multiple images to achieve higher resolution like other super-resolution techniques.[1] Our system employs birefringent crystals in order to multiplex the measurement.

In a conventional system, it would not easily be possible to discern between two point source locations that both image to the same pixel. The birefringent crystal will help break this ambiguity by imaging a point source to multiple locations on the detector. Using a crossed set of two birefringent crystals, four impulses can be imaged from a single point source.[2] Ensuring that the distance between these imaged points is not an integer number of the pixel size will increase the information obtained from a single exposure.[3,4] Even if one point source is imaged to an Airy disc falling completely within a detector pixel, by varying the shift created by the birefringent crystal, the other copies of the point source's image can be engineered to cross pixel boundaries.

In this paper, we use the pixel intensity values as weightings, and propose that the center of mass of the four impulses will estimate the relative location of a point source on the detector. We will show that the accuracy of this calculation will be better than the nominal pixel size.

2. Experimental Setup

A Roper Scientific CoolSnap cf CCD was used to capture the images. This camera has an array of 1392x1040 pixels, each of size 4.65x4.65 µm. Two quartz crystals, each approximately 5mm thick, were placed directly upon the focal plane in series. The crystal axes were orientated at approximately 45 degrees to each other in order to provide maximum displacement of the generated impulses. Together these crystals generate a complex impulse response when incident with unpolarized light. A polarized point source would not produce the same impulse response as an unpolarized source. However, if polarization of a source remains consistent, localization should still be possible, although the resolution may not be as fine. A Nikon 50 mm f/1.8 lens was attached to the camera body. The imaging system remained stationary thought the experiment.

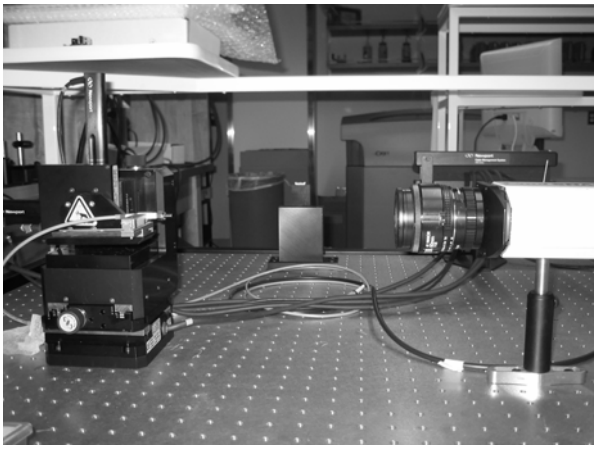

Fig. 1: Photograph of experimental setup

Coupled from with a white light source, an optical fiber with 8 µm mode diameter was mounted 25 cm away from the camera lens. This tip was translated perpendicular to the optical axis by two computer controlled Newport VP-25XA stages. These stages

have a resolution of 0.1 µm. Sample captured images are shown in Figure 2. Exposure times of 1 ms were used throughout the experiment. The magnification of the system was approximately 0.23.

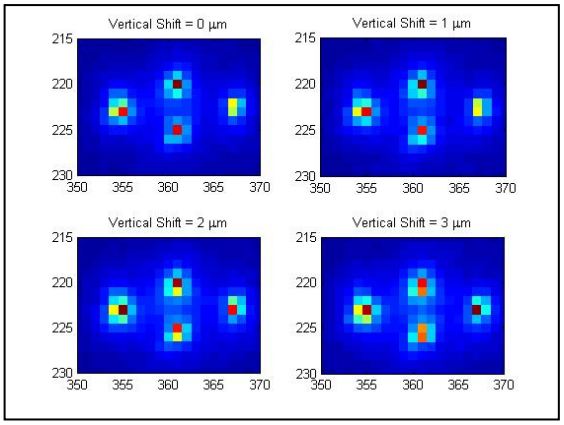

Fig. 2: Four images captured sequentially. Observe the variation of the intensity distribution of the rightmost impulse.

3. Algorithm

The algorithm employed estimates the location of a point source by calculating the center of mass of its image using pixel intensities as weightings. However, before this estimation is calculated, raw pixel values were preprocessed in the following manor to minimize the effects of detector noise.

First, the the mean (µ) and standard deviation (σ) of pixel values were calculated for each image. The formulas for these quantities are as follows:

$$\mu = \frac{1}{M}\sum_{i=1}^{n}\sum_{j=1}^{m} D_{ij} \qquad (1.1)$$

and

$$\sigma^2 = \frac{1}{M}\sum_{i=1}^{n}\sum_{j=1}^{m} (D_{ij} - \mu)^2 \qquad (1.2)$$

where $M = \sum_{i=1}^{n}\sum_{j=1}^{m} D_{ij}$ and D_{ij} is the pixel intensity at location (i, j).

Then, a threshold was set at µ+6σ. Any pixel value below this threshold was set to zero. Thus, small background fluctuations did not affect the outcome of the center of mass calculation. Equations 1.3 and 1.4 summarize the center of mass calculation used to obtain the approximate relative location of the point source image.

$$x_{cm} = \frac{1}{M}\sum_{i=1}^{n}\sum_{j=1}^{m} iD_{ij} \qquad (1.3)$$

and

$$y_{cm} = \frac{1}{M}\sum_{i=1}^{n}\sum_{j=1}^{m} jD_{ij} \qquad (1.4)$$

4. Experimental Results

Mounted on the computer controlled translation stage, the fiber tip was stepped in increments of 0.5 µm recording an image at each of 50 locations. The images were preprocessed, and the coordinates of the center of mass were calculated in units of pixels. The coordinates of the first captured image (r_o, c_o) was used as a reference location for the remaining images. The Cartesian distance was calculated for each location using equation (1.5).

$$\Delta d_i = P\sqrt{(r_i - r_o)^2 + (c_i - c_o)^2} \qquad (1.5)$$

where P is the detector pixel size.

A linear regression was performed on the data set shown in Figure 3, and the distance from this line is shown in Figure 4.

The estimation for the location of the image is very well approximated by the center of mass algorithm. The algorithm is not adding a bias to the measurement; the mean error deviation from the linear regression was far less than 1 pm. The standard deviation of the distances between the calculated point source locations to the best fit line was calculated to be 0.170 µm, which more than 25 times smaller than the pixel size of 4.65µm.

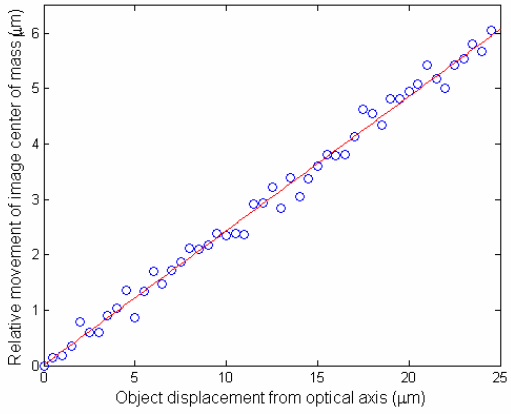

Fig. 3: Narrow field calculated relative movement vs object position from initial location. The object was stepped in equal increments of 0.5 µm.

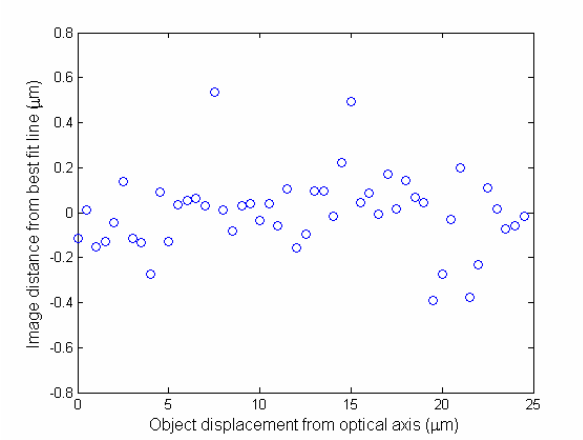

Fig. 4: Narrow field estimation error from linear regression on detector plane. Pixel size is 4.65 µm.

A more appropriate metric to characterize system performance is the angular resolution. This can be calculated from the standard deviation of error in linear localization on the detector plane, the system magnification and object distance. Using the slope of the linear regression performed in Figure 3, we calculate the magnification of the system to be 0.233. Therefore, a detector plane uncertainty of 0.170 µm, translates to an uncertainty of 0.729 µm in object space. The calculated angular resolution of the system is 2.91 microradians.

A similar experiment was performed utilizing the full detector plane in order to determine if the subpixel resolution can be maintained across the camera's full field of view. The physical thickness of the two crystals limited the minimum distance between the camera lens and the focal plane. This constrains the camera's field of view to 6.4 degrees.

The fiber was stepped in increments of 500 µm from an on axis location to a point imaging to the edge of the focal plane.

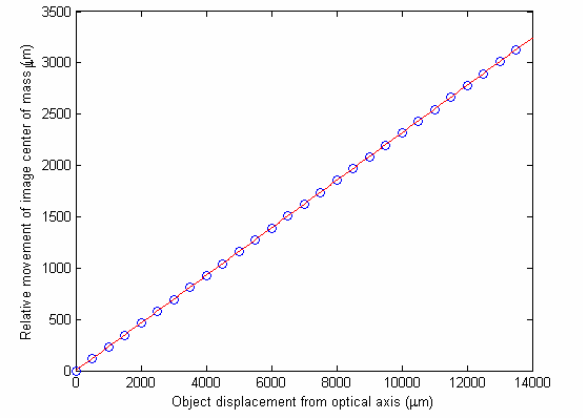

Fig. 5: Full field calculated relative movement vs object position from initial location. The object was stepped in equal increments of 500 µm.

As before, for each data point, the error distance from this best fit line was calculated. The algorithm, as before, added negligible bias. A larger standard deviation of the errors was calculated to be 0.316 µm. The slope of the best fit line for the full field scan differed only in the third significant figure from the on axis scan. For this data, a magnification of 0.232 minimizes mean square error. Using these parameters, an uncertainty of 1.36 µm can be derived. System angular resolution is calculated to be 5.44 microradians. With a field of view of .112 radians, the instrument developed has the ability to distinguish between approximately 20,000 unique object locations in one dimension.

5. Conclusion

We have demonstrated that using the first moment of the pixel intensity distribution localizes a point source to a finer accuracy than the pixel pitch. The critical element in this system is the crossed birefringent crystals. This component achieves super-resolution in a single static measurement; no scanning is required.

As shown, this technique can be used to localize a point source, but can be expanded to provide super-resolved information about a more complex object or even multiple objects.

The development of a more sophisticated algorithm may yield an improvement in system resolution. With better knowledge of the impulse response and the pixel sampling function, a more advanced model can be implemented. It should be possible to use an iterative gradient based algorithm to estimate location. In practice, noise will limit performance.

The presented technique for the localization of a source on a detector demonstrates a resolution improvement over the conventional use of the focal plane array.

6. References

[1] S. C. Park, M.K. Park, and M. G. Kang, "Super-resolution image reconstruction: a technical overview," IEEE Signal Processing Magazine, 20, 21-36 (2003).

[2] B.E.A. Saleh and M.C. Teich, *Fundamentals of Photonics*, John Wiley & Sons, New York, pp. 210-223, 1991.

[3] J.P. Fillard, H. Mtimet, J.M. Lussert, M. Castagne, "Computer-Simulation of Superresolution Point-Source Image Detection," Optical Engineering 32 (11):2936-4, Nov 1993.

[4] B.F. Alexander, "Elimination of Systematic-Error In Subpixel Accuracy Centroid Estimation," Optical Engineering 30 (9): 1320-1331, Sep 1991.